



First-principles study of the magnetic anisotropic exchange interactions and magnetoelastic coupling in Fe-based kagome metals

Surasree Sadhukhan ^{*}, Bishal Thapa , and I. I. Mazin 

*Department of Physics and Astronomy, [George Mason University](#), Fairfax, Virginia 22030, USA
and Quantum Science and Engineering Center, [George Mason University](#), Fairfax, Virginia 22030, USA*



(Received 25 February 2025; revised 30 September 2025; accepted 1 October 2025; published 20 October 2025)

Anisotropic magnetic exchange interactions induced by spin-orbit coupling have been less explored than their isotropic part and, when they were, they were nearly always limited to the Dzyaloshinskii-Moriya interaction (DMI) and single-site anisotropy. In our work, we address the full magnetic exchange interaction matrix using density functional theory, including all terms allowed by the crystal symmetry of Fe-based kagome metal. To this end, we propose an accurate but computationally inexpensive protocol to obtain the anisotropic magnetic exchange interactions, whereby only the spin quantization axis is rotated and other parameters remain fixed, reducing computational noise. We observe a smooth trigonometric energy dependence on the rotation angle and extract magnetic interaction parameters from the trigonometric equation fitting obtained from our mathematical expression for the Fe-based kagome metal. We also investigated how the chemical composition and crystal structure affect DMI and other anisotropic terms in the Fe-based kagome structure. Our simple protocol for robust calculations of nonzero anisotropic magnetic interactions, which naturally cancel our systematic errors, can be readily applied to other materials. In the second part, we calculate zone-center phonon frequencies and show how they depend on the presence of magnetism and on the pattern of magnetic ordering.

DOI: [10.1103/x14h-fbxm](https://doi.org/10.1103/x14h-fbxm)

I. INTRODUCTION

Investigating the interplay of magnetic exchange interactions in the presence of spin-orbit coupling (SOC), and lattice properties, offers exciting potential for revealing unique physical phenomena in magnetism. Typically, the Heisenberg model describes magnetic exchange interactions without SOC [1,2] (albeit in metals often interactions beyond Heisenberg, such as biquadratic, are non-negligible); however, there exist multiple classes of magnetic phenomena that cannot be described by a Heisenberg Hamiltonian alone. This may be as simple as magnetic anisotropy of rather involved like Kitaev interactions [3,4], dual spin liquids [5,6], skyrmions [7–9], weak ferromagnetism in antiferromagnetic materials, and so on. It is essential to have prior knowledge of the anisotropic component of the magnetic exchange interaction. Certain noncollinear magnetic materials, including MnSi [10], YbMgGaO₄ [11], MnPS₃ [12], LiCu₂O₂ [13], etc., demonstrate magnetic properties with significant contributions from the off-diagonal anisotropic part of the symmetric (as opposed to DMI) magnetic exchange interaction. In a nutshell, anisotropic exchange plays a key role in shaping the magnetic behavior of a material and its sensitivity to external stimuli like pressure, temperature, doping, etc. A convenient approach to expressing the general spin Hamiltonian is to represent it as the sum of nonrelativistic, i.e., rotationally invariant, terms, such as Heisenberg and, occasionally, biquadratic [14] or even ring exchange [15], while anisotropic (i.e., not rotationally invariant) contributions are limited to antisymmetric DMI and single-ion anisotropy (SIA) at individual sites [16]. It is worth

noting that while DMI, formally, is the only contribution that appears in the first order in SOC [16], the same is not true for SIA and, as long as the latter is included, all elements of the 3×3 matrix of the exchange interactions must be assessed. This is very rarely done and, if it is done, it is usually not done on a model level (e.g., Hubbard model), not from the first principles DFT calculations [17]. Experimental probes of spin dynamics, e.g., inelastic neutron scattering, routinely fit the measured spin wave spectra with the Heisenberg + DMI + SIA Hamiltonians [11,18], though even on this experimental level SIA and anisotropic exchange can manifest themselves differently [19]. In this paper, we have proposed a simple and computationally rather inexpensive, but surprisingly accurate method to determine all the matrix elements of the magnetic exchange matrix, including, but not limited to DMI and SIA by deriving first the most general expression compatible with the crystal symmetry and then applying to the first principles density functional theory. The high accuracy of our approach is assured by the fact that each fitting involves a fixed magnetic pattern, while the spin quantization axis is rotated (as implemented in, for instance, the VASP package [20,21]). This ensures elimination of many systematic errors and improves the accuracy enormously. As an example we consider well-studied Fe-based kagome binaries, FeSn and FeGe (in the latter case, neglecting the low-temperature charge density wave). The Fe-based kagome lattice, with its corner-sharing triangular network of magnetic ions, provides a compelling test case due to its intriguing magnetic and topological properties. Also, these materials have been extensively studied [22–24]. We have observed that the DM interaction for FeGe is reported to be around 0.03 meV [25]. However, in our analysis, we found the z component of the DM interaction

^{*}Contact author: ssadhukh@gmu.edu

to be approximately 0.77 meV [which emerges at second order in the spin-orbit coupling (SOC) within the framework of the SOC included Hubbard Hamiltonian]. Furthermore, we explore how chemical composition and crystallographic structure impact the DMI and other magnetic interactions and found that the effect is significant. This inspired us to look at the opposite effect: influence of magnetic ordering on the lattice properties, such as phonon frequencies.

II. CALCULATION METHODOLOGY

We calculated the electronic structure of two Fe-based kagome lattices using first-principles density functional theory (DFT). The calculations employed a plane-wave basis set with a 500 eV energy cutoff and PAW pseudopotentials as implemented in the Vienna *ab initio* simulation package (VASP) [20,21]. The Perdew–Burke–Ernzerhof (PBE) formulation of the generalized gradient approximation (GGA) [26] was chosen for exchange-correlation effects. For Fe we used the Fe_pv potential with *p*-states included as valence and Sn_d and Ge_d for the anions. Convergence tests with respect to the *k*-point density were performed with the in-plane meshes up to 19, and out-of-plane up to 18 points, and the difference in the results was used to establish the computational inaccuracy. In order to assure the only the quantization axis is rotated (which is important for ensuring that the total energy is a simple trigonometric function) we applied directional constraint as implemented in VASP. In addition, we calculated zone-center phonon modes. For these calculations we used the *k* mesh of $18 \times 18 \times 11$ and fully optimized the internal positions with the force convergence criterion of 0.001 eV/Å.

III. CRYSTAL STRUCTURE

The antiferromagnetic 2D kagome metals FeX (X = Ge, Sn) crystallize in a hexagonal structure with the space group *P6/mmm* (no. 191), where the honeycomb layer of X₂ in 2*d* Wyckoff positions alternate with the triangular Fe₃X layers, with Fe in 3*f* Wyckoff positions forming a kagome lattice and X filling the 1*a* centers of Fe hexagons. There are no free internal parameters, so the lattice is fully characterized by the two lattice parameters *a* and *c* (see Table I). Here, we focus on a single 2D kagome layer of Fe to calculate the single-site and the nearest-neighbor magnetic interactions. The lattice parameters for FeGe and FeSn are *a* = 4.9658 Å and 5.2970 Å, respectively, with corresponding *c*-axis parameters *c* = 4.0399 Å and 4.4810 Å. Even though the 3D group *P6/mmm* is centrosymmetric, the inversion centers are located between the kagome layers. An individual Fe₃X layer retains however important symmetry elements of this space group, namely *M_x*, *M_y*, and *M_z*, which play a key role in defining the mathematical form of the anisotropic exchange matrix.

IV. DERIVATION OF THE MAGNETIC HAMILTONIAN AND THE EFFECT OF THE QUANTIZATION AXIS ROTATION

The most general expression of the bilinear magnetic interaction in the presence of spin-orbit coupling reads

$$H = \sum_{i,j} \mathbf{S}_i \cdot \hat{J}_{ij} \cdot \mathbf{S}_j + \sum_i \mathbf{S}_i \cdot \hat{K}_{ii} \cdot \mathbf{S}_i, \quad (1)$$

TABLE I. Crystallographic information for different magnetic patterns—nonmagnetic (NM), ferromagnetic (FM), and antiferromagnetic (AFM)—along with the corresponding Wyckoff positions and space groups, both under zero unilateral strain and perturbative unilateral strain.

| Magnetic pattern | Wyckoff position | | Space group |
|------------------|-------------------|----------|--------------------|
| | Element | Site | |
| NM/FM/AFM | Fe | <i>f</i> | 191, <i>P6/mmm</i> |
| | Sn | <i>d</i> | |
| | Sn | <i>a</i> | |
| AFM | Unilateral strain | | 65, <i>Cmmm</i> |
| | Fe | <i>b</i> | |
| | Fe | <i>e</i> | |
| | Sn | <i>j</i> | |
| | Sn | <i>a</i> | |

where summation is over all sites *i* and all bonds *ij*. Here

$$\hat{J}_{ij} = \begin{pmatrix} J_{xx} & J_{xy} & J_{xz} \\ J_{yx} & J_{yy} & J_{yz} \\ J_{zx} & J_{zy} & J_{zz} \end{pmatrix}, \quad \hat{K}_{ij} = \begin{pmatrix} K_{xx} & K_{xy} & K_{xz} \\ K_{yx} & K_{yy} & K_{yz} \\ K_{zx} & K_{zy} & K_{zz} \end{pmatrix}$$

are the exchange interaction between two spins *S_i* and *S_j* and the second-order single-site anisotropy, respectively. The point to be noted here is that *S_i* and *S_j* represent the spin vector with three components along *X*, *Y*, and *Z* directions. The Hamiltonian (1) must be invariant under crystal symmetry operation, which acts upon the indices *i*, *j* and (only the point group) upon the spins *S_i*. For a hexagonal point group *6/mmm* the only admissible elements of the *K̂* matrix are *K_{xx}* = *K_{yy}* and *K_{zz}* or, removing the gauge constant, one meaningful number, *K* = *K_{zz}* − *K_{xx}*. Now, a general exchange matrix *Ĵ* can be decomposed into a diagonal matrix whose trace gives the Heisenberg exchange,

$$\begin{pmatrix} J_H - J_z/2 - J_y & 0 & 0 \\ 0 & J_H - J_z/2 + J_y & 0 \\ 0 & 0 & J_H + J_z \end{pmatrix},$$

where *J_z* and *J_y* represent Ising exchange and *XY* exchange, a symmetric off-diagonal matrix

$$\begin{pmatrix} 0 & J_{xy} & J_{zx} \\ J_{xy} & 0 & J_{yz} \\ J_{zx} & J_{yz} & 0 \end{pmatrix},$$

which is sometimes called compass exchange, and an anti-symmetric part

$$\begin{pmatrix} 0 & J_{xy} & -J_{zx} \\ -J_{xy} & 0 & J_{yz} \\ J_{zx} & -J_{yz} & 0 \end{pmatrix} = \begin{pmatrix} 0 & D_z & -D_y \\ -D_z & 0 & D_x \\ D_y & -D_x & 0 \end{pmatrix}$$

is DMI with the axial DM vector *D*.

During the symmetry analysis of the crystal structure, the combined application of the mirror plane *M_z* (*x* ↦ −*x*, *y* ↦ −*y*, *z* ↦ *z*) and the mirror plane *M_x* (*x* ↦ *x*, *y* ↦ −*y*, *z* ↦ −*z*) enforces the conditions *J_{zx}* = *J_{xz}* = 0 and *J_{yz}* = *J_{zy}* = 0, thereby diminishing these

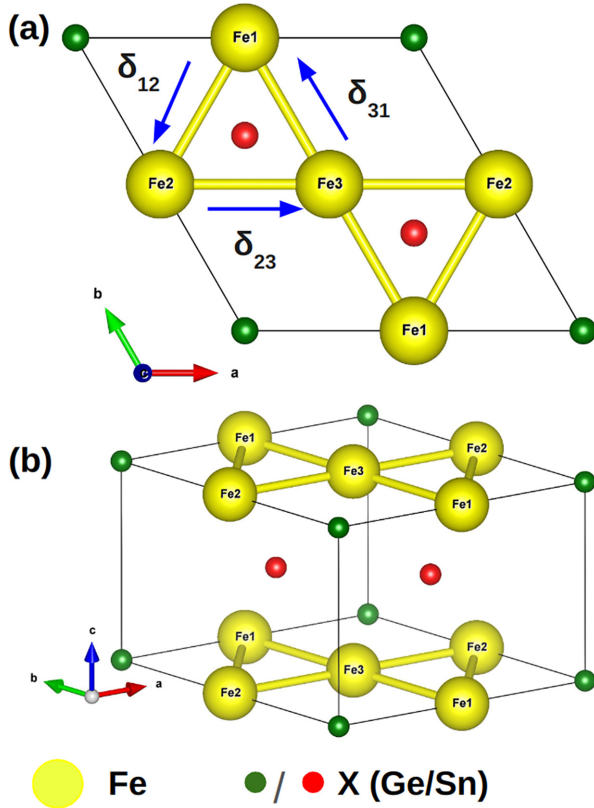


FIG. 1. Crystal structure of FeX ($X = \text{Ge}, \text{Sn}$). Fe atoms are represented by yellow spheres, X atoms in the X_2 layer by red spheres, and X atoms in the Fe_2X layers by the green ones. The arrows correspond to the ordering selected for the bonds labeled as δ 's.

elements of the exchange interaction matrix. Next the element of the puzzle is the threefold rotational axis C_{3z} passing through the red balls in Fig. 1. It rotates the 23 bond into the 31 one and acts upon the spins as the standard R_{3z} rotational matrix,

$$R_{3z} = \begin{pmatrix} -1/2 & -\sqrt{3}/2 & 0 \\ \sqrt{3}/2 & -1/2 & 0 \\ 0 & 0 & 1 \end{pmatrix}, \quad \mathbf{S} \rightarrow R_{3z} \cdot \mathbf{S}.$$

Applying this operation to Eq. (1), we observe that

$$\begin{pmatrix} J_{xx} & a + d_z & 0 \\ a - d_z & J_{yy} & 0 \\ 0 & 0 & J_{zz} \end{pmatrix} = \begin{pmatrix} \frac{\sqrt{3}(J_{xx}+J_{yy})}{4} - \frac{a\sqrt{3}}{2} & \frac{\sqrt{3}(J_{xx}-J_{yy})}{4} - \frac{a}{2} + d_z & 0 \\ \frac{\sqrt{3}(J_{xx}-J_{yy})}{4} + \frac{a}{2} - d_z & \frac{\sqrt{3}(J_{xx}+J_{yy})}{4} + \frac{a\sqrt{3}}{2} & 0 \\ 0 & 0 & J_{zz} \end{pmatrix} \quad (2)$$

from which it follows that $a = 0$, $J_{xx} = J_{yy} = J_H$, and $J_{zz} = J_H + J_z$. Thus the final form of the magnetic exchange matrix is

$$\hat{J}_{23} = \hat{J}_{31} = \hat{J}_{12} = \begin{pmatrix} J_H & d_z & 0 \\ -d_z & J_H & 0 \\ 0 & 0 & J_H + J_z \end{pmatrix} \quad (3)$$

and the total energy per unit cell, E , will be

$$\begin{aligned} \frac{E}{2} = & \mathbf{d} \cdot (\mathbf{S}_2 \times \mathbf{S}_3 + \mathbf{S}_3 \times \mathbf{S}_1 + \mathbf{S}_1 \times \mathbf{S}_2) \\ & + J_H (\mathbf{S}_2 \cdot \mathbf{S}_3 + \mathbf{S}_3 \cdot \mathbf{S}_1 + \mathbf{S}_1 \cdot \mathbf{S}_2) \\ & + J_z (S_{2z}S_{3z} + S_{3z}S_{1z} + S_{1z}S_{2z}) \\ & + \frac{K}{2} (S_{2z}^2 + S_{3z}^2 + S_{1z}^2), \end{aligned} \quad (4)$$

where J_H is the nonrelativistic Heisenberg exchange and J_z characterizes the XY (or z -Ising) exchange. The three spin vectors, \mathbf{S}_1 , \mathbf{S}_2 , and \mathbf{S}_3 , correspond to the Fe1, Fe2, and Fe3 atoms, respectively, while \mathbf{d} represents the DMI vector. Each spin vector can be expressed in components as $\mathbf{S}_1 = (S_{1x}, S_{1y}, S_{1z})$, with a similar notation for $\mathbf{S}_2 = (S_{2x}, S_{2y}, S_{2z})$ and $\mathbf{S}_3 = (S_{3x}, S_{3y}, S_{3z})$.

To extract all parameters in the above equation, we will construct two spin arrangements that we will rotate rigidly. In the first case, the directions of spin magnetic moments of Fe1, Fe2, and Fe3 are set as the X , Y , and Z Cartesian axes (X is parallel to the δ_{23} bond) and the spin quantization axis is rotated about the Y axis by an angle ϕ . The resulting equation is given by

$$E = 2d_z(\cos \phi - \sin \phi) - J_z \sin 2\phi + K. \quad (5)$$

Note that K cannot be determined from this operation since it simply shifts the energy zero and the Heisenberg part falls out entirely. In the second case we set the Fe spin all parallel to Z and the quantization axis is rotated about the Y axis by an angle ϕ . The resulting equation becomes

$$E = 6J_H + 3J_z + \frac{3}{2}K + 3(J_z + K) \cos 2\phi. \quad (6)$$

Since J_H is much larger than all other terms, the two energies are, in the first approximation, shifted by $6J_H$, which gives us an opportunity to extract J_H even if the non-relativistic ferrimagnetic calculations cannot be converged (as is the case, for instance, for FeGe) and the variation with the angles lets us extract independently d_z , J_z , and $J_z + K$.

A. First principles calculation of the exchange matrix

We performed first-principles DFT calculations using the GGA + SOC, as described above. By keeping all computational parameters constant except for the rotation angle, we minimized the computational noise and eliminate systematic errors. As a result, the calculated dependencies, despite the very small energy scales, fit exceedingly well Eqs. (5) and (6), as illustrated in Figs. 2(a)–2(d), demonstrating the high quality of the nearest-neighbor approximation used in the previous section. We applied this methodology to two Fe-based kagome metals, FeGe and FeSn, chosen due to the extensive studies on Fe-based kagome systems and due to their simple 2D crystal structure [22–24]. In the case of FeGe, both the isotropic and anisotropic exchange interactions have been reported [25]. For FeSn, although its Heisenberg isotropic magnetic exchange interactions have been previously investigated [27,28], a comprehensive understanding of its anisotropic exchange parameters remains absent in the literature. Considering the rich magnetic behav-

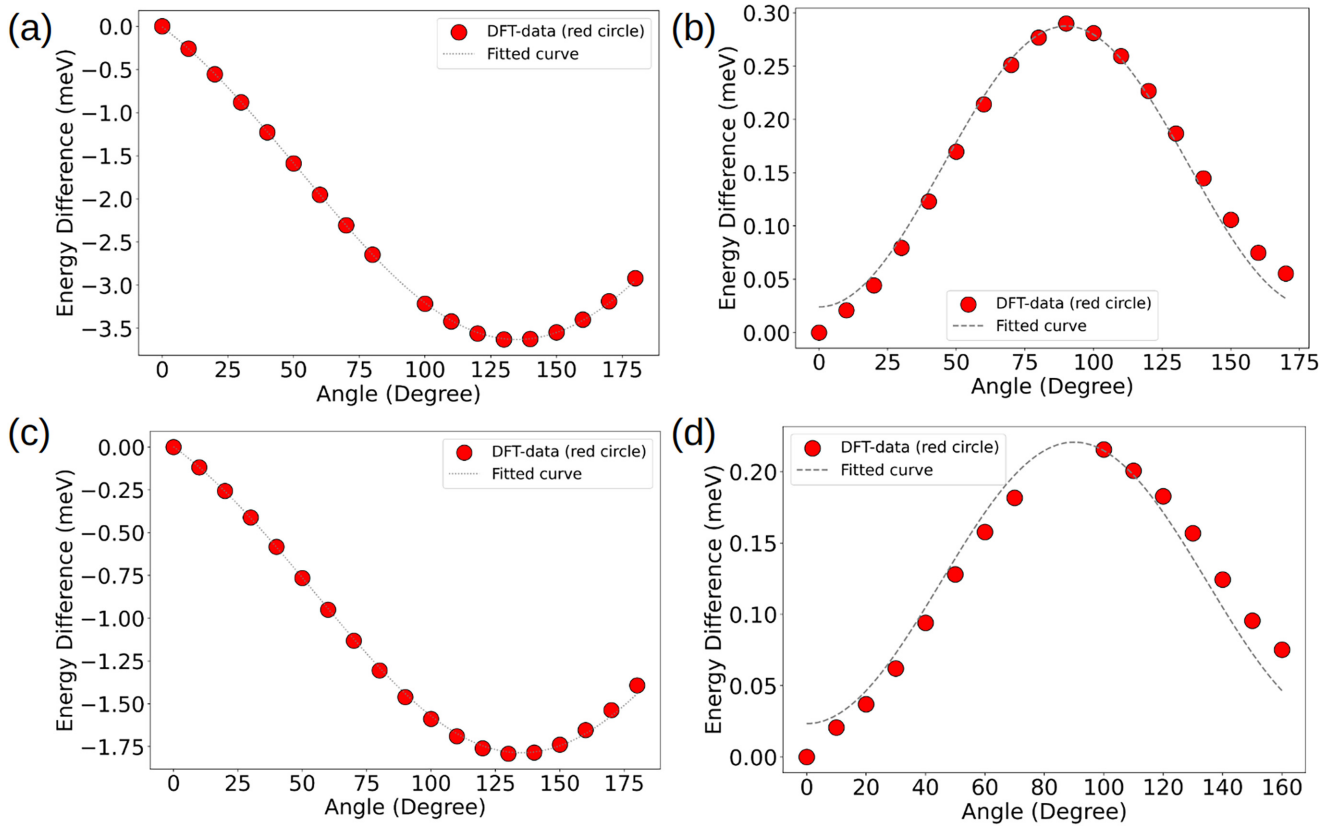


FIG. 2. Calculated total energy difference per unit cell of FeX (X = Ge, Sn) as a function of the rotation angle of the spin quantization axis. The rotation is around the Cartesian Y direction. The direction of spin magnetic moments of Fe1, Fe2, and Fe3 atoms are constrained parallel to (a) along X, Y, and Z, respectively, and in (b) along Z for all atoms for FeGe. Panels (c) and (d) show the same for FeSn. The k mesh is $19 \times 19 \times 15$. Note the high quality of the trigonometric fits to Eqs. (5) and (6).

ior of FeSn, it is essential to thoroughly explore its exchange parameters.

Now first, for the case of FeGe, the calculated matrix elements are provided in Supplemental Table I [29]. To ensure convergence of the exchange parameters, we tested various k -point meshes, with energy variations as a function of the rotation angle illustrated in Supplemental Figs. S1 and S2 [29] for FeGe (plotted in three different k mesh). The isotropic exchange interaction is -43.05 ± 0.2 meV, which is consistent with previously calculated first principles theoretical outcome [25,30]. Our analysis revealed that the Z component

of the DMI, d_z , is approximately 0.77 ± 0.08 meV, significantly larger than the previously reported value of ~ 0.03 meV using both magnetic force theorem combined with linear response approach, which is unusually small for a 3d transition metal. The Ising exchange parameter J_z was determined to be approximately -0.06 ± 0.02 meV (here and below the error bars indicate the level of convergence with respect to the k mesh). Furthermore, we identified a single-site anisotropy of 0.02 meV, which is consistent with existing experimental data [31]. The complete anisotropic exchange matrix elements, expressed in meV, are as follows (with the fitting errors):

$$J_{\alpha\beta}[\text{FeGe}_{\text{FeGe}}] = (-43.05 \pm 0.2)\delta_{\alpha\beta} + \begin{pmatrix} 0 & 0.77 \pm 0.08 & 0 \\ -0.77 \pm 0.08 & 0 & 0 \\ 0 & 0 & -0.06 \pm 0.02 \end{pmatrix}. \quad (7)$$

Our other test case, FeSn, was selected because it is isoelectronic and isostructural with FeGe, with the only difference being in the values of a and c and replacing Ge with the isoelectronic Sn. We note that less data on magnetic exchange parameters is currently available in the literature. We employed a similar computational protocol. Again, we found that the trigonometric Eqs. (5) and (6) described the energy

variation followed exceedingly well, as illustrated in Figs. 2(c) and 2(d). We found that for FeSn $d_z \approx 0.36 \pm 0.1$ meV, $J_z \approx -0.04 \pm 0.01$ meV, and $K \approx 0.01$ meV. The isotropic nonrelativistic exchange we found to be $J \approx -64.78 \pm 0.01$ meV, which is also consistent with reported data where first-principles density functional theory calculations are employed to determine the Heisenberg interactions; however,

the results show a noticeable deviation from the experimental values [27,28]. The complete form of the magnetic exchange matrix in the presence of spin-orbit coupling is given by

$$J_{\alpha\beta}[\text{FeSn}_{\text{FeSn}}] = (-64.78 \pm 0.01)\delta_{\alpha\beta} + \begin{pmatrix} 0 & 0.36 \pm 0.1 & 0 \\ -0.36 \pm 0.1 & 0 & 0 \\ 0 & 0 & -0.04 \pm 0.01 \end{pmatrix}. \quad (8)$$

It is instructive to compare the two. For instance, DMI in FeGe is two times larger than in FeSn and the same is true by the two other relativistic terms—despite the fact that Sn is much heavier. What is the reason for that—the chemical substitution or the structural difference? To answer this question, we added to our two real materials two hypothetical ones: FeGe in the FeSn crystal structure ($\text{FeGe}_{\text{FeSn}}$) and FeSn in the FeGe crystal structure ($\text{FeSn}_{\text{FeGe}}$), as depicted in Figs. S5(a) and S5(d) of the Supplemental Material [29], which represents Eqs. (5) and (6) for both the cases. The results were as follows: for $\text{FeGe}_{\text{FeSn}}$, we found that J_z changes moderately from ≈ -0.04 to ≈ -0.14 meV, but d_z changes dramatically, even flipping the sign, from $\approx +0.73$ to ≈ -0.85 meV. We also verified that d_z changes smoothly between these two values, as the structure is gradually changed from that of FeGe to that of FeSn, passing through zero in between. We have also found the isotropic nonrelativistic exchange to be ≈ -75.92 meV, which is nearly the isotropic term in the $\text{FeSn}_{\text{FeSn}}$ setup [cf. Eqs. (8)] and single site anisotropy is 0.05 meV. Thus, in our first hypothetical scenario, when the FeGe crystal structure is substituted with FeSn, the full exchange matrix is (we drop the fitting error here and below)

$$J_{\alpha\beta}[\text{FeGe}_{\text{FeSn}}] = -75.92 \cdot \delta_{\alpha\beta} + \begin{pmatrix} 0 & -0.85 & 0 \\ 0.85 & 0 & 0 \\ 0 & 0 & -0.20 \end{pmatrix}. \quad (9)$$

When, conversely, the crystal structure of FeGe was used with the chemical composition of FeSn, d_z remained positive, and grew to ≈ 1.38 meV, while the Ising term J_z was slightly reduced to -0.024 meV. We have also determined that the isotropic nonrelativistic exchange is approximately -46.60 meV, very close to the nonrelativistic term in FeGe compounds, as shown in Eqs. (7), while the single-site anisotropy is -0.03 meV. Hence, in the second hypothetical scenario, where the FeSn crystal structure is replaced with FeGe, the exchange matrix is given in meV as

$$J_{\alpha\beta}[\text{FeSn}_{\text{FeGe}}] = -46.60\delta_{\alpha\beta} + \begin{pmatrix} 0 & 1.38 & 0 \\ -1.38 & 0 & 0 \\ 0 & 0 & -0.02 \end{pmatrix}. \quad (10)$$

These findings indicate that the bond geometry plays a more important role in this kagome systems than the strength of the SOC on ligands, as opposed, for instance to the famous

CrI_3 – CrBr_3 – CrCl_3 series. In particular, the lattice contraction when going from the FeSn structure to the FeGe one leads to systematic increase in the value (not absolute value) of d_z by 1–1.6 meV, while replacing Ge by Sn leads to an increase by 0.6–1.2 meV. Given that there clearly are negative as well as positive contributions, the absolute value of the DMI interaction may not show any clear trend.

In addition to the total DM interaction described above in terms of d , we have separately calculated the first- (d_1) and second-order (d_2) DMI values using our proposed methodology. To determine d_1 and d_2 , we consider a supercell configuration. In our case, a $2 \times 1 \times 1$ supercell along the X direction is employed, as shown in Supplemental Fig. S6(a) [29]. We adopt a nonlinear spin configuration where the spin orientations for the six sites of Fe from S_1 to S_6 are given as \hat{X} , \hat{Y} , \hat{X} , $-\hat{Z}$, \hat{X} , and $-\hat{Z}$, respectively. For this configuration, the resulting energy expression is

$$E = E_0 + 2d_2(\cos \phi + \sin \phi), \quad (11)$$

where E_0 is a constant and ϕ denotes the rotation angle of the spin quantization axis. From Eq. (11), the parameter d_2 is extracted based on the trigonometric dependence of energy as we have done for unit cell configurations. The obtained average values are $d_2 = -0.173 \pm 0.002$ meV for FeGe and $d_2 =$

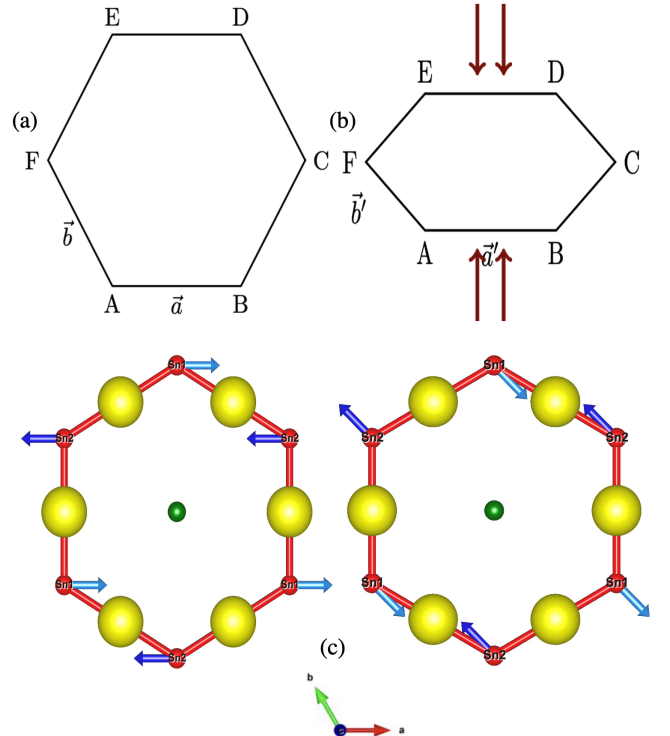


FIG. 3. For a hexagonal lattice, (a) and (b) depict schematics for $\epsilon = 0$ and $\epsilon > 0$, respectively, illustrating symmetry reduction resulting from the application of unilateral strain. While the volume of the hexagonal crystal remains constant, the orientation of the hexagonal plane changes. Additionally, (c) showcases the doubly degenerate E_{2g} quadrupolar mode of the Sn ($2d$ position) plane, with arrow indicating positions displaced due to the applied strain. The figures show the ab plane, while the c axis is perpendicularly out of the paper.

TABLE II. Optical phonon modes for distinct magnetic states, with frequencies in cm^{-1} . Modes listed in the last column only are the zone-boundary [$\mathbf{q} = (0, 0, 1/2)$] modes. The Raman-active mode is highlighted in bold.

| S. no. | Optical mode | | | |
|--------|----------------------------|--------------|----------------|--------------------|
| | Irreducible representation | Non-magnetic | Ferro-magnetic | Antiferro-magnetic |
| 1 | E_{1u} | 213.9 | 254.4 | 246.9 |
| 2 | A_{2u} | 223.8 | 244.6 | 248.2 |
| | E_{1u} | | | 244.7 |
| | B_{1u} | | | 238.8 |
| | E_{2u} | | | 238.2 |
| | B_{2u} | | | 232.7 |
| 3 | B_{2u} | 150.4 | 239.6 | 230.0 |
| 4 | B_{1u} | 194.4 | 191.8 | 202.1 |
| 5 | E_{2u} | 137.2 | 183.7 | 200.5 |
| | A_{2u} | | | 194.9 |
| | A_{1g} | | | 160.5 |
| 6 | E_{1u} | 131.6 | 164.2 | 157.5 |
| 7 | B_{2g} | 150.5 | 158.3 | 156.9 |
| 8 | E_{2g} | 153.2 | 152.0 | 156.6 |
| | E_{1u} | | | 144.5 |
| | E_{2u} | | | 142.8 |
| | B_{1u} | | | 99.9 |
| 9 | A_{2u} | 105.2 | 88.3 | 95.0 |
| | E_{1g} | | | 84.3 |
| 10 | E_{1u} | 130.3 | 85.6 | 83.8 |
| | A_{2u} | | | 78.1 |
| | E_{1u} | | | 58.5 |

-0.46 ± 0.02 meV for FeSn, as summarized in Table 4 of the Supplemental Material [29]. The convergence of d_2 with respect to both in-plane and out-of-plane \mathbf{k} points has been verified (Table 4). Based on these results, the first-order parameter is determined as $d_1 = -0.597 \pm 0.01$ meV for FeGe and $d_1 = 0.08 \pm 0.02$ meV for FeSn. The corresponding trigonometric fits of the energy are shown in Figs. S6(b) and S6(c) for FeGe and FeSn, respectively. The high quality of these fits within a small energy scale ensures the reliability of the extracted DMI interaction values.

B. Raman spectroscopy of FeSn

Given the strong effect of the structure on magnetic interaction, it is instructive to investigate the opposite, the effect of magnetism on lattice properties, especially such that can

be easily addressed by the experiment. Zone center and, especially, Raman phonons provide the desirable probe. FeGe forms, at low temperature, a charge density wave [30,32], so we have concentrated on FeSn in this study. Specifically, we performed the calculations in a locally nonmagnetic case (local magnetization on Fe fully suppressed), ferromagnetic, and A-type antiferromagnetic (ferromagnetic planes stacked antiferromagnetically). The latter is the ground state in the calculations. Spin-orbit interaction (SOI) was not included in the calculations, as it is not expected to affect the phonon frequency in light elements such as Fe and Sn. We used the optimized structure to calculate the phonon mode for the nonmagnetic (NM) and ferromagnetic (FM) pattern, which contains six atoms per unit cell. Meanwhile, the antiferromagnetic (AFM) pattern involved doubling of the unit cell and a total of 12 atoms per unit cell. In the NM calculations, the magnetic moment is suppressed on each Fe, while the FM calculations converged to magnetic moments of $2.05 \mu_B$ per Fe. The total magnetization per Fe is slightly smaller, $1.93 \mu_B$, due to small induced polarization of the opposite sign on Sn ($\sim -0.1 \mu_B$), an effect known in other contexts as Schrieffer-Wolff interaction (see, e.g., Ref. [33]). In the AFM calculations, the magnetic moment of Fe and the Sn residing in the Fe plane is basically unchanged, while the interplanar Sn has zero magnetization by symmetry. The crystal structure details are tabulated in Table I for the magnetophonon calculation along with the application of volume conserving unilateral strain.

We systematically investigated the magnetophonon coupling in the FeSn by introducing magnetic interactions within the unit cell. Only one doubly degenerate Raman-active mode is allowed, E_{2g} , which involves only lateral displacements of the $2d$ Sn shown in Fig. 3(c). Note that the antiferromagnetic case requires doubling of the unit cell along c . This normally leads to zone-boundary modes with $\mathbf{q} = (0, 0, \pi/c)$ to be tagged as the zone center, even though they remain Raman-forbidden (unless magnetic ordering is accompanied by a charge order). These zone center modes are listed in Table II.

In order to address possible magnetoelastic coupling, we have also calculated the Raman modes under the in-plane uniaxial volume-confirming strain. The latter reduces the symmetry to orthorhombic ($Cmmm$, no. 65), as shown schematically in Fig. 3. Note that, while the compressive case in this case is not the same as the tensile strain, the difference arises only because the x (100) direction is not exactly equivalent to the y (210) direction and the difference is of the higher order in strain.

TABLE III. Intensities for Raman active mode before and after the application of unilateral strain for antiferromagnetic magnetic pattern. The degenerate Raman active mode, E_{2g} , splits into A_g and B_{1g} and the previously silent mode, B_{2g} , splits into Raman active mode B_{3g} .

| AFM coupling without strain | | AFM coupling with unilateral strain | | | | | |
|-----------------------------|---------------------------------|-------------------------------------|---------------------------------|-------|-------|-------|-------|
| Symmetry | Wave number (cm ⁻¹) | Symmetry | Wave number (cm ⁻¹) | | | | |
| species | ϵ = 0 | species | ϵ → | 1% | −1% | 2% | −2% |
| E _{2g} | 156.6 | A _g | | 158.6 | 152.9 | 161.2 | 150.3 |
| E _{2g} | 156.6 | B _{1g} | | 152.9 | 158.1 | 149.6 | 160.4 |
| B _{2g} | 156.9 | B _{3g} | | 156.5 | 156.5 | 156.0 | 156.3 |

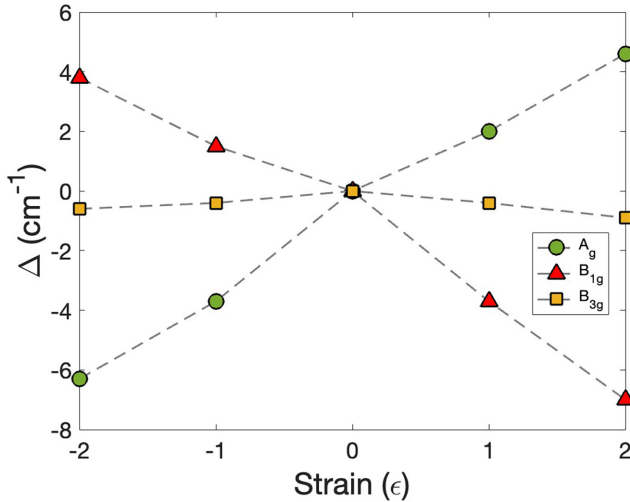


FIG. 4. Change of selected zone-center phonons (for other modes, see the Supplemental Material [29]) as a function of uniaxial strain ϵ (in %) applied along the Fe-Fe bond. The notations are given as pertaining to the undistorted structure, i.e., the E_{2g} modes split (linearly in ϵ) into A_g and B_{1g} (active in different polarizations) and the silent B_{2g} mode shifts (quadratically in ϵ) and acquires a Raman intensity proportional (also quadratically).

In Cartesian coordinates, a strain ϵ corresponds to the transformation matrix for the lattice vector of

$$\mathcal{R}' = \begin{pmatrix} (1 + \epsilon) & 0 & 0 \\ -\frac{1}{2}(1 + \epsilon) & \frac{\sqrt{3}}{2} \frac{1}{1 + \epsilon} & 0 \\ 0 & 0 & 1 \end{pmatrix}.$$

This symmetry lowering opens up (quadratically in ϵ) Raman activity for previously inactive modes, as well as splits and shifts of the original E_{2g} mode. Specifically, the latter splits into A_{1g} and B_{1g} modes and the original silent B_{2g} mode, corresponding to vertical shifts of the Sn_2 planes with respect to the Fe_3Sn planes, becomes the B_{3g} Raman-active mode (Table III). We observe that the strongest effect of strain is splitting of the main E_{2g} mode (Fig. 4).

We also performed first principle calculations on the same system, assuming different magnetic states for Fe: locally nonmagnetic and ferro- or antiferromagnetically ordered. We also find that suppressing the local magnetic moment on Fe leads to a considerable error in the phonon modes (up to 45 cm^{-1} in the case of the E_{1u} mode, which is pure Fe). A similar effect was observed, for instance, in Ref. [34], but not on the same scale. Even more interesting, we find that the magnetic order couples strongly with some phonons, with up to 17 cm^{-1} shifts. This is an exceptionally strong magnetophonon coupling and may be related to the unusual kagome geometry.

V. SUMMARY AND CONCLUSION

In this study, we have investigated the anisotropic magnetic exchange interactions in an Fe-based kagome metal. We proposed a straightforward and computationally efficient method to determine all elements of the magnetic exchange matrix using a trigonometric fitting approach based on the energy variation as a function of the magnetization-rotation angle. Applying our method to a well-studied Fe-based kagome structure, we derived an analytic expression for the energy variation with respect to the rotational angle. Our first-principles calculations demonstrate excellent agreement with this analytic form, even at a finer energy scale (meV). Compared to existing methods, our approach provides a relatively accurate determination of the magnetic exchange matrix in the low-energy regime. Notably, our methodology can separately identify the single-site anisotropy and the Ising exchange term, an issue not addressed in previous literature. Overall, our work serves as a valuable guide for deriving analytic expressions in conjunction with first-principles calculations to efficiently obtain magnetic exchange matrices. As anticipated, the antisymmetric Dzyaloshinskii-Moriya interaction, which appears in the first order of spin-orbit coupling (SOC), is significantly smaller than the isotropic exchange interaction. However, it is notably more extensive than the symmetric isotropic terms, which only emerge in the second order of the Hubbard Hamiltonian. Since the Dzyaloshinskii-Moriya (DM) interaction arises due to spin-orbit coupling, the ratio of the DM interaction to the Heisenberg interaction $|\frac{D}{J}|$ is expected to be small. Our results, with values of 0.017 for FeGe and 0.005 for FeSn, align well with this expectation. We have also determined the first-order (d_1) and second-order (d_2) Dzyaloshinskii-Moriya interactions for both FeGe and FeSn. In these calculations we found that the exchange interactions dramatically depend on the structural environment. This motivated us to investigate, in addition, an opposite effect, namely, the effect of magnetic order on lattice dynamics. To this end, we have calculated Raman active modes in different magnetic configurations and found a rather large dependence.

ACKNOWLEDGMENTS

This work was supported by the National Science Foundation under Award No. DMR-2403804. We also acknowledge support from QSEC and computational resources from the Hopper HPC cluster at GMU. The crystal structure visualizations presented in this work were prepared using the VESTA software package [35].

DATA AVAILABILITY

No data were created or analyzed in this study.

- [1] N. D. Mermin and H. Wagner, Absence of ferromagnetism or antiferromagnetism in one- or two-dimensional isotropic Heisenberg models, *Phys. Rev. Lett.* **17**, 1133 (1966).
- [2] S. Katsura, Statistical mechanics of the anisotropic linear Heisenberg model, *Phys. Rev.* **127**, 1508 (1962).

- [3] H. Liu, J. Chaloupka, and G. Khaliullin, Kitaev spin liquid in 3D transition metal compounds, *Phys. Rev. Lett.* **125**, 047201 (2020).
- [4] S. M. Winter, A. A. Tsirlin, M. Daghofer, J. v. d. Brink, Y. Singh, P. Gegenwart, and R. Valentí, Models and materials for

- generalized Kitaev magnetism, *J. Phys.: Condens. Matter* **29**, 493002 (2017).
- [5] P. A. Maksimov, Z. Zhu, S. R. White, and A. L. Chernyshev, Anisotropic-exchange magnets on a triangular lattice spin waves, accidental degeneracies, and dual spin liquids, *Phys. Rev. X* **9**, 021017 (2019).
- [6] L. Savary and L. Balents, Quantum spin liquids a review, *Rep. Prog. Phys.* **80**, 016502 (2017).
- [7] A. Fert, N. Reyren, and V. Cros, Magnetic skyrmions advances in physics and potential applications, *Nat. Rev. Mater.* **2**, 17031 (2017).
- [8] K. E. -Sitte, J. Masell, R. M. Reeve, and M. Kläui, Perspective: Magnetic skyrmions—Overview of recent progress in an active research field, *J. Appl. Phys.* **124**, 240901 (2018).
- [9] N. Nagaosa and Y. Tokura, Topological properties and dynamics of magnetic skyrmions, *Nat. Nanotechnol.* **8**, 899 (2013).
- [10] V. Borisov, Y. O. Kvashnin, N. Ntallis, D. Thonig, P. Thunström, M. Pereiro, A. Bergman, E. Sjöqvist, A. Delin, L. Nordström *et al.*, Heisenberg and anisotropic exchange interactions in magnetic materials with correlated electronic structure and significant spin-orbit coupling, *Phys. Rev. B* **103**, 174422 (2021).
- [11] X. Zhang, F. Mahmood, M. Daum, Z. Dun, J. A. M. Paddison, N. J. Laurita, T. Hong, H. Zhou, N. P. Armitage, and M. Mouriagal, Hierarchy of exchange interactions in the triangular-lattice spin liquid YbMgGaO_4 , *Phys. Rev. X* **8**, 031001 (2018).
- [12] T. Olsen, Magnetic anisotropy and exchange interactions of two-dimensional FePS_3 , NiPS_3 and MnPS_3 from first principles calculations, *J. Phys. D: Appl. Phys.* **54**, 314001 (2021).
- [13] Z. Seidov, T. P. Gavrilova, R. M. Eremina, L. E. Svistov, A. A. Bush, A. Loidl, and H. A. Krug von Nidda, Anisotropic exchange in LiCu_2O_2 , *Phys. Rev. B* **95**, 224411 (2017).
- [14] A. L. Wysocki, K. D. Belashchenko, and V. P. Antropov, Consistent model of magnetism in ferropnictides, *Nat. Phys.* **7**, 485 (2011).
- [15] Y. N. Huang, H. O. Jeschke, and I. I. Mazin, CrRhAs: a member of a large family of metallic kagome antiferromagnets, *npj Quantum Mater.* **8**, 32 (2023).
- [16] T. Moriya, Anisotropic superexchange interaction and weak ferromagnetism, *Phys. Rev.* **120**, 91 (1960).
- [17] T. Yildirim, A. B. Harris, A. Aharony, and O. Entin-Wohlman, Anisotropic spin Hamiltonians due to spin-orbit and Coulomb exchange interactions, *Phys. Rev. B* **52**, 10239 (1995).
- [18] B. Hälgl and A. Furrer, Anisotropic exchange and spin dynamics in the type-I (-IA) antiferromagnets CeAs, CeSb, and USb: A neutron study, *Phys. Rev. B* **34**, 6258 (1986).
- [19] N. J. Ghimire, R. L. Dally, L. Poudel, D. C. Jones, D. Michel, N. T. Magar, M. Bleuel, M. A. McGuire, J. S. Jiang, J. F. Mitchell *et al.*, Competing magnetic phases and fluctuation-driven scalar spin chirality in the kagome metal YMn_6Sn_6 , *Sci. Adv.* **6**, eabe2680 (2020).
- [20] G. Kresse and J. Hafner, *Ab initio* molecular dynamics for liquid metals, *Phys. Rev. B* **47**, 558(R) (1993).
- [21] G. Kresse and J. Furthmüller, Efficient iterative schemes for *ab initio* total-energy calculations using a plane-wave basis set, *Phys. Rev. B* **54**, 11169 (1996).
- [22] M. Kang, L. Ye, S. Fang, J. S. You, A. Levitan, M. Han, J. I. Facio, C. Jozwiak, A. Bostwick, E. Rotenberg *et al.*, Dirac fermions and flat bands in the ideal kagome metal FeSn, *Nat. Mater.* **19**, 163 (2020).
- [23] Y. Xie, L. Chen, T. Chen, Q. Wang, Q. Yin, J. R. Stewart, M. B. Stone, L. L. Daemen, E. Feng, H. Cao *et al.*, Spin excitations in metallic kagome lattice FeSn and CoSn, *Commun. Phys.* **4**, 240 (2021).
- [24] Z. Lin, C. Wang, P. Wang, S. Yi, L. Li, Q. Zhang, Y. Wang, Z. Wang, H. Huang, Y. Sun *et al.*, Dirac fermions in antiferromagnetic FeSn kagome lattices with combined space inversion and time-reversal symmetry, *Phys. Rev. B* **102**, 155103 (2020).
- [25] H. Zhou, S. Yan, D. Fan, D. Wang, and X. Wan, Magnetic interactions and possible structural distortion in kagome FeGe from first-principles calculations and symmetry analysis, *Phys. Rev. B* **108**, 035138 (2023).
- [26] J. P. Perdew, K. Burke, and M. Ernzerhof, Generalized gradient approximation made simple, *Phys. Rev. Lett.* **77**, 3865 (1996).
- [27] Y. F. Zhang, X. S. Ni, T. Datta, M. Wang, D. X. Yao, and K. Cao, *Ab initio* study of spin fluctuations in the itinerant kagome magnet FeSn, *Phys. Rev. B* **106**, 184422 (2022).
- [28] S. H. Do, K. Kaneko, R. Kajimoto, K. Kamazawa, M. B. Stone, J. Y. Y. Lin, S. Itoh, T. Masuda, G. D. Samolyuk, E. Dagotto *et al.*, Damped Dirac magnon in the metallic kagome antiferromagnet FeSn, *Phys. Rev. B* **105**, L180403 (2022).
- [29] See Supplemental Material at <http://link.aps.org/supplemental/10.1103/x14h-fbxxm> for the trigonometric fitting curves of the energy difference as a function of the rotation angle for FeGe and FeSn, obtained using different k -meshes, in order to determine the magnetic exchange parameters.
- [30] X. Teng, D. W. Tam, L. Chen, H. Tan, Y. Xie, B. Gao, G. E. Granroth, A. Ivanov, P. Bourges, B. Yan *et al.*, Spin-charge-lattice coupling across the charge density wave transition in a kagome lattice antiferromagnet, *Phys. Rev. Lett.* **133**, 046502 (2024).
- [31] J. Bernhard, B. Lebech, and O. Beckman, Magnetic phase diagram of hexagonal FeGe determined by neutron diffraction, *J. Phys. F: Met. Phys.* **18**, 539 (1988).
- [32] H. Miao, T. T. Zhang, H. X. Li, G. Fabbri, A. H. Said, R. Tartaglia, T. Yilmaz, E. Vescovo, J. X. Yin, S. Murakami *et al.*, Signature of spin-phonon coupling driven charge density wave in a kagome magnet, *Nat. Commun.* **14**, 6183 (2023).
- [33] J. K. Glasbrenner, I. Žutić, and I. I. Mazin, Theory of Mn-doped II-II-V semiconductors, *Phys. Rev. B* **90**, 140403(R) (2014).
- [34] D. Reznik, K. Lokshin, D. C. Mitchell, D. Parshall, W. Dmowski, D. Lamago, R. Heid, K. P. Bohnen, A. S. Sefat, M. A. McGuire *et al.*, Phonons in doped and undoped BaFe_2As_2 investigated by inelastic x-ray scattering, *Phys. Rev. B* **80**, 214534 (2009).
- [35] K. Momma and F. Izumi, VESTA 3 for three-dimensional visualization of crystal, volumetric and morphology data, *J. Appl. Crystallogr.* **44**, 1272 (2011).